Fulminant lung fibrosis in non-resolvable COVID-19 requiring transplantation

Soma S. K. Jyothula,[a,b,i] Andrew Peters,[c,i] Yafen Liang,[d] Weizhen Bi,[c] Pooja Shivshankar,[c] Simon Yau,[e] Puneet S. Garcha,[f] Xiaoyi Yuan,[d] Bindu Akkanti,[a,b] Scott Collum,[c] Nancy Wareing,[c] Rajarajan A. Thandavarayan,[e] Fernando Poli de Frias,[f] Ivan O. Rosas,[f] Bihong Zhao,[g] L. Maximilian Buja,[g] Holger K. Eltzschig,[d] Howard J. Huang,[e] and Harry Karmouty-Quintana[a,b,h,*]

[a]Department of Internal Medicine, McGovern Medical School, University of Texas Health Science Center at Houston, Houston, TX, USA
[b]Center for Advanced Cardiopulmonary Therapies and Transplantation at UTHealth/McGovern Medical School, Houston, TX, USA
[c]Department of Biochemistry and Molecular Biology, McGovern Medical School, University of Texas Health Science Center at Houston, Houston, TX, USA
[d]Department of Anesthesiology, McGovern Medical School, University of Texas Health Science Center at Houston, Houston, TX, USA
[e]Houston Methodist DeBakey Transplant Center, Houston Methodist Hospital, Houston, TX, USA
[f]Department of Medicine, Pulmonary, Critical Care and Sleep Medicine, Baylor College of Medicine, Houston, TX, USA
[g]Department of Pathology and Laboratory Medicine, McGovern Medical School, University of Texas Health Science Center at Houston, Houston, TX, USA
[h]UTHealth Pulmonary Center of Excellence, McGovern Medical School, University of Texas Health Science Center at Houston, Houston, TX, USA

eBioMedicine
2022;86: 104351
Published Online XXX
https://doi.org/10.1016/j.ebiom.2022.104351

Summary

Background Coronavirus Disease 2019 (COVID-19) can lead to the development of acute respiratory distress syndrome (ARDS). In some patients with non-resolvable (NR) COVID-19, lung injury can progress rapidly to the point that lung transplantation is the only viable option for survival. This fatal progression of lung injury involves a rapid fibroproliferative response and takes on average 15 weeks from initial symptom presentation. Little is known about the mechanisms that lead to this fulminant lung fibrosis (FLF) in NR-COVID-19.

Methods Using a pre-designed unbiased PCR array for fibrotic markers, we analyzed the fibrotic signature in a subset of NR-COVID-19 lungs. We compared the expression profile against control lungs (donor lungs discarded for transplantation), and explanted tissue from patients with idiopathic pulmonary fibrosis (IPF). Subsequently, RT-qPCR, Western blots and immunohistochemistry were conducted to validate and localize selected pro-fibrotic targets. A total of 23 NR-COVID-19 lungs were used for RT-qPCR validation.

Findings We revealed a unique fibrotic gene signature in NR-COVID-19 that is dominated by a hyper-expression of pro-fibrotic genes, including collagens and periostin. Our results also show a significantly increased expression of Collagen Triple Helix Repeat Containing 1(CTHRC1) which co-localized in areas rich in alpha smooth muscle expression, denoting myofibroblasts. We also show a significant increase in cytokeratin (KRT) 5 and 8 expressing cells adjacent to fibroblastic areas and in areas of apparent epithelial bronchiolization.

Interpretation Our studies may provide insights into potential cellular mechanisms that lead to a fulminant presentation of lung fibrosis in NR-COVID-19.

Funding National Institute of Health (NIH) Grants R01HL154720, R01DK122796, R01DK109574, R01HL133900, and Department of Defense (DoD) Grant W81XWH2110032 to H.K.E. NIH Grants: R01HL138510 and R01HL157100, DoD Grant W81XWH-19-1-0007, and American Heart Association Grant: 18IPA34170220 to H.K.-Q. American Heart Association: 19CDA34660279, American Lung Association: CA-622265, Parker B. Francis Fellowship, 1UL1TR003167–01 and The Center for Clinical and Translational Sciences, McGovern Medical School to X.Y.

Keywords: Extracorporeal life support; ECMO; Periostin (POSTN); Extracellular matrix; Post-acute SARS-CoV-2 sequelae (PASC); CTHRC1; KRT5; KRT8

*Corresponding author. 6431 Fannin Street, Suite 6.214, Houston, TX 77030.
E-mail address: Harry.Karmouty@uth.tmc.edu (H. Karmouty-Quintana).
[i]Contributed equally.

Research in context

Evidence before this study

A devastating complication of COVID-19 is the continuation of severe pulmonary sequelae following SARS-CoV-2 infection. We have termed this non-resolvable (NR)- COVID-19. These conditions can aggravate to the point that patients require a lung transplant.

Added value of this study

Using 23 NR-COVID-19 lung explants, we revealed an increase in fibrotic gene expression in NR-COVID-19 comparable to idiopathic pulmonary fibrosis (IPF), the most common diagnosis for lung transplantation. Our studies also revealed an increased number of cellular markers for CTHRC1, KRT5, and KRT8 positive cells in NR-COVID-19 that were of similar magnitude to IPF.

Implications of all the available evidence

These results underscore the aggressive fibrotic nature following SARS-CoV-2 infection. Specifically, our data points at the heightened presence of CTHRC1 expressing cells which are highly pro-fibrotic in additional to KRT5 and particularly KRT8 signals in bronchiolized areas of the epithelium in NR-COVID-19. These findings are important at understanding the cellular mechanisms that promote lung fibrosis following viral infection.

Introduction

Coronavirus disease 2019 (COVID-19) is caused by severe acute respiratory syndrome coronavirus 2 (SARS-CoV-2) infection. Over 617 million cases and 6.5 million deaths have been reported globally (https://coronavirus.jhu.edu/ accessed October 1, 2022). The majority of COVID-19 patients develop mild symptoms. However, around 5% will experience severe symptoms including acute respiratory distress syndrome (ARDS).[1–5] ARDS is characterized by acute hypoxemic respiratory failure with bilateral pulmonary infiltrates.[6–10] ARDS is treated by eliminating the underlying causes, and supportive care including ventilatory and non-ventilatory strategies.[11–13]

Although a lung-protective ventilation strategy has improved the long-term pulmonary outcomes of ARDS patients, lung fibrosis significantly contributes to morbidity and mortality.[14] Lung injury in ARDS along with other risk factors such as aging and mechanical ventilation contribute to alveolar injury and the deposition of the extracellular matrix (ECM). Like other diseases caused by coronavirus such as SARS-CoV and Middle East respiratory syndrome (MERS) Co–V, fibrotic changes in the lung have also been observed in patients suffering from COVID-19 associated ARDS.[15–17] *In vitro* studies suggest that SARS-CoV-2 infection leads to increased expression of profibrotic factors such as transforming growth factor (TGF) -B1 and fibronectin (FN1) in lung epithelial cells.[18] A recent study has also identified an expansion of Collagen Triple Helix Repeat Containing 1 (CTHRC1) expressing cells in the lungs of patients who succumbed to COVID-19 ARDS.[19] This is significant since CTHRC1+ cells were first identified in fibrotic lungs and are concentrated within fibroblastic foci.[20] These studies also reported increased expression of cytokeratin (KRT)-8 expressing cells and commitment to a lineage expressing KRT-5.[20] Intriguingly, in an experimental model of bleomycin-induced fibrosis, transitional cells expressing KRT8 have been implicated in the progression of pulmonary fibrosis.[21] Similarly, KRT5 expressing cells have been shown to play a decisive role in epithelial lung repair.[22] Despite this, the primary cellular/molecular mechanisms of fibrosis in COVID-19 remains unclear. This is of particular importance as a subset of patients with ARDS develop fulminant lung fibrosis (FLF) that requires lung transplantation.[23,24] Despite similarities observed between COVID-19 patients requiring lung transplantation and idiopathic pulmonary fibrosis (IPF),[23,25] the fulminant development of lung fibrosis in non-resolvable COVID-19 (NR-COVID-19) patients, underscores a unique and aggressive fibroproliferative mechanism. In this study, our main objective was to identify the molecular and cellular changes associated with NR-COVID-19. Herein, we evaluated the expression levels of profibrotic genes from lung samples of up to 23 patients who underwent lung transplantation due to NR-COVID-19 and compared them to lung tissues derived from donor lungs discarded for transplantation that served as controls. Remarkably, our studies demonstrate that explanted lungs from patients with NR-COVID-19 present with high expression of fibrotic genes, particularly collagens and periostin, increased presence of CTHRC1+ cells and an overwhelming expression of KRT-8 cells, consistent with evidence of bronchiolization in the parenchyma.

Methods

Ethics: human studies

The use of human material for this study was reviewed by the Committee for the Protection of Human Subjects at The University of Texas Health Science Center at Houston (HSC-MS-15-1049 and HSC-MS-08-0354),

Houston Methodist Hospital (Pro00003392) and Baylor College of Medicine (H-46823). Explanted lung tissue from patients undergoing lung transplantation due to NR-COVID-19 (TXC#) or Idiopathic Pulmonary Fibrosis (IPF#) was processed on site within 60 min. Discarded donor lungs for transplantation served as controls (CTRL#) and were obtained from LifeGift Organ Procurement (Houston, TX). Lung tissues were collected from the mid portion of the upper and lower lobes as described previously.[26] The details of the NR-COVID-19 study population are summarized in Table 1, and for control and IPF lung tissue in Supplementary Table S1. Control and IPF samples were age, sex and ethnicity matched as closely as possible to our NR-COVID-19 cohort. Informed consent from all participants was obtained. Sex was self-reported. Since 83% (19 out of 23) patients who underwent lung transplantation due to NR-COVID-19 were male; IPF and control groups were enriched for male subjects.

Quantitative RT-PCR and PCR array

Total RNA was isolated from frozen lung tissue using the Qiagen MiniKit (Germantown, MD). RNA was purified and treated using RNase-free DNase (ArcticZymes Tromso, Norway). The predesigned Prime PCR array for pulmonary fibrosis (H384) for SYBR Green from Bio-Rad (Hercules, CA) was used. The PCR array was run following the manufacturer's instructions, the raw data will be made available. Individual primers for validation RT-PCR are described in Supplementary Table S2 and were run using SYBR Green.

Immunoblots and ELISA

Western blots were performed by isolating protein in RIPA buffer (Alfa Aesar, J63306) with protease and phosphatase inhibitor (Thermo-Fisher, 78440). Protein concentration was measured by BCA assay (Pierce, 23227). Proteins were mixed with 6X SDS buffer (Boston Bioproducts, BP-111R) and heated to 95 Celsius for

Sample ID	Age	Sex	Ethnicity	Comorbidities	Invasive mechanical ventilation/ECMO	COVID specific treatments	Day of transplant from positive PCR
TXC1	69	M	H	HTN, DM II	No	Convalescent plasma, dexamethasone, remdesivir	57
TXC2	63	M	C	HTN	No	Convalescent plasma, dexamethasone, remdesivir	68
TXC3	46	F	H	None	No	Dexamethasone	139
TXC4	52	M	H	None	Yes/Yes	Convalescent plasma, dexamethasone, remdesivir	90
TXC5	16	M	H	None	Yes/Yes	Convalescent plasma, dexamethasone, remdesivir, IVIG	127
TXC6	42	F	H	Thrombotic Thrombocytopenic Purpura on Rituxan	Yes/Yes	Dexamethasone, remdesivir	86
TXC7	33	M	C	HTN	Yes/Yes	Convalescent plasma, dexamethasone, remdesivir	180
TXC8	24	M	C	None	Yes/Yes	Dexamethasone, remdesivir	55
TXC9	53	M	H	DM II, HTN, HLD, Obesity	No/Yes	Dexamethasone, remdesivir, convalescent plasma	143
TXC10	40	M	H	None	Yes/Yes	Remdesivir, convalescent plasma, dobutamine, NO, epoprostenol	106
TXC11	43	M	H	DM II, HTN, Morbid Obesity	Yes/Yes	Remdesivir, convalescent plasma, dexamethasone, levaquin	74
TXC12	54	M	AA	None	Yes/Yes	Remdesivir, dexamethasone, Azithromycin	110
TXC13	60	M	H	HTN	Yes/Yes	Dexamethasone	143
TXC14	37	M	AA	HTN, DM II	Yes/Yes	Remdesivir, dexamethasone	126
TXC15	34	M	As.	None	Yes/Yes	Dexamethasone, convalescent plasma	189
TXC16	42	M	H	Obesity, dyslipidemia	Yes/Yes	Remdesivir, dexamethasone	146
TXC17	63	M	H	GERD, Hypothyroidism, allergies, Previous hospitalization for COVID w/ Discharge	Outpatient	Monoclonal antibodies, remdesivir, dexamethasone, azithromycin/ rocephin	211
TXC18	58	M	H	DM, HTN	No/No	Convalescent plasma, dexamethasone, remdesivir	N/A
TXC19	32	M	H	Obesity	Yes/Yes	Convalescent plasma, dexamethasone, remdesivir, Ruxolitnib	N/A
TXC20	55	M	H	Obesity, CAD, anxiety, DM II, HTN, HLD	No/No	Decadron, remdesivir, convalescent plasma	91
TXC21	60	F	C	Obesity, HTN, HLD, DM II, anxiety, GERD	No/No	Convalescent plasma RemDex, steroids	136
TXC22	47	F	C	None	Yes/Yes	Steroids, remdesivir, tocilizumab, baricitinib	57
TXC23	52	M	C	Smoking, heroin, RB-ILD	Yes/Not	Uncertain	168
Average	46.7						119

All the patients underwent lung transplantation between July 2020 and July 2021. Hospital course was best established in 19 of the 23 patients. We recorded demographics and treatment for our study. AA = African American, As. = Asian, C = Caucasian, H = Hispanic When available, mean time from PCR positivity to lung transplant was recorded (range 55–211). Hypertension (HTN), diabetes mellitus type two (DM II), hyperlipidemia (HLD), gastroesophageal reflux disease (GERD), coronary artery disease (CAD), respiratory bronchiolitis-interstitial lung disease (RB-ILD).

Table 1: **List of transplant patients from our cohort.**

5 min. Samples were ran on 4–20% gradient gels (Bio-rad, 4568096) or 10% gels (Bio-rad, 4561033) and transferred using Bio-rad Trans-Blot Turbo (Bio-rad, 1701274). Membranes were blocked with 5% milk in TBST (Sigma, T9039) for 1hr and probed with the primary antibody overnight. Blots were washed with TBST and incubated with a secondary antibody (CellSignalin, 7074S) for 1hr. Bio-rad Clarity ECL was used and blots were imaged using the Bio-rad ChemiDoc Touch. Membranes were stripped using Restore WB Stripping Buffer (Thermo Scientific, 21059) for 15 min and re-blocked with 5% milk in TBST. The GAPDH primary, secondary, and imaging were then performed as above on the same membrane as each protein of interest. Each image was also taken as white light illuminated to merge with the luminescence image to allow for visualization of the protein ladder in the included images of full Western blot membranes. Total protein isolated from frozen lung tissue was incubated with primary antibodies against CTHRC1, cytokeratin (KRT)5, KRT8, periostin (POSTN); versican (VCAN), pSMAD 2, 3; SMAD 2,3; pSMAD 1,5,9; SMAD1, ID1 using Glyceraldehyde 3-phosphate dehydrogenase (GAPDH) as a loading control. The experimental conditions are described in Supplementary Table S3.

Histology and immunohistochemistry (IHC) staining

Formalin-fixed paraffin embedded lung samples were cut at 5 μm thickness and stained for Masson's Trichome, Ashcroft scores were performed by investigators blinded to group status as previously described.[26] Dual IHC for KRT5 and SMA, KRT8 and SMA, and CTHRC1 and SMA were performed and slides were mounted with cytoseal. Experimental details are described in Supplementary Table S3.

Statistics

All data was checked for outliers using the ROUT test. An un-paired two-tailed Mann–Whitney t-test was performed for data comprising two groups. One-way ANOVAs with the Benjamini, Krieger and Yekutieli post-hoc tests were performed for grouped data. GraphPad Prism 9.0 or higher was used to analyse the data. Sample size was determined based on previous studies using human samples from our group.[26] Samples were randomized and assigned a new number to permit investigators to be blinded to group status. Inclusion and exclusion criteria: for IPF and NR-COVID-19 groups, only explanted lung tissues from patients undergoing lung transplantation were utilized. For control lung samples, only lung tissues from discarded donors with no history of acute or chronic pulmonary disease were used. IPF and control samples did not have a positive history for COVID-19.

Role of funders

Funding agencies did not have a role in the collection, analysis, and interpretation of data; in the writing of the report; and in the decision to submit the article for publication.

Results

Clinical characteristics of the COVID-19 patients that underwent a lung transplant

The clinical course, Computed Tomography (CT), and pathological findings of the twenty-three patients for which we have a more detailed clinical history included in the study are described in Tables 1 and 2. A thorough description of each individual transplant recipient is supplied in the supplemental information. All patients were approved for transplantation following approval from the institutional transplant medical review board.

In summary, this cohort of patients is from Houston, TX, USA, a known COVID-19 hotspot in 2020 through 2021, but, as a tertiary care center includes the surrounding area. Of our cohort, all the patients underwent lung transplantation between July 2020 and July 2021. Of the patients for which we had a more established hospital course, 96% of patients received steroids (dexamethasone) and 70% received remdesivir. Convalescent plasma therapy was provided to 57% of patients per existing practice at that time. About 70% were placed on invasive mechanical ventilation or ECMO prior to transplant. This unique cohort of patients exhibits persistent pulmonary impairment with profound hypoxemia with a prolonged hospital course and multiple in hospital complications. Some of the patients required multiple other interventions or multiple organ transplantation. Our cohort represents a unique and fulminant course of NR-COVID-19 that required lung transplantation. They had a mean age of 47 and included a patient as young as 16-years-old.

Radiological findings were not available for all patients. Table 2 indentified diffuse ground glass opacities (GGO) with bronchiectasis in a majority of patients. For example, TXC6 had pneumatocles that were likely secondary to ventilator associated injury. TXC7 showed extensive consolidations and was on ECMO support for more than 30 days prior to CT Chest. TXC3 showed bilateral basal honeycombing similar to a usual interstitial pneumonia (UIP) pattern. TXC2 was an ex-smoker and had emphysema on his CT Chest. The radiological findings mimic interstitial lung disease (ILD) specifically a non-specific interstitial pneumonia (NSIP) pattern. Multiple patients had the stigmata of ARDS cystic lung destruction.

Histopathological evaluation of explanted lungs revealed diffuse alveolar damage (DAD) with overlapping acute, organizing, or fibrotic phases in most cases. Microscopic honeycombing was noted in multiple NR-COVID subjects. Significant chronic interstitial inflammation was noted in all patients. TXC1 had

CASE no.	CT Chest High resolution	Histopathology
TXC1	Diffuse Ground glass opacities (GGO) Reticulations. Septal thickening. Traction bronchiectasis. Consolidations in upper lobes	Extensive cystic degeneration of the lung parenchyma, probably secondary to ischemic cause. Elastin stain highlights the thick intima of a middle-sized pulmonary artery. Fibrotic pleura with mild chronic inflammation noted.
TXC2	Diffuse GGO, Reticulations, Septal thickening. Basal predominant Traction bronchiectasis. Centrilobular and Paraseptal emphysema	Relatively less affected area with well-preserved lung architecture but increased cellularity in alveolar wall, consistent with cellular non-specific interstitial pneumonia (NSIP) pattern of injury. Interstitial emphysema with histiocytic infiltrate and numerous multinucleated giant cells. More advanced fibrosis.
TXC3	Bilateral sub pleural GGO. Diffuse bronchiectasis/Bronchiolectatsis. Lower lobe honeycombing. Scattered tiny pulmonary nodules.	Diffuse alveolar septal thickening with fibrosis, consistent with fibrotic NSIP pattern of injury. Early honeycombing and dilated pulmonary artery without thickening of the wall. Dilated vasculature without significant thickening of the wall.
TXC4	Bilateral GGO. Septal Thickening. Diffuse bronchiectasis.	Diffuse alveolar damage (DAD) with organizing features. Extensive microscopic honey combing. Mild uniform fibrosis. Few arteries show vasculopathy with hypertrophied walls with significant luminal narrowing.
TXC5	Bilateral GGO. Cystic Changes in bilateral upper lobes. Consolidative changes in basal lower lobes.	DAD with organizing features. Focal mature fibrosis. Emphysema and Pneumatoceles. Diffuse chronic interstitial inflammation.
TXC6	Bilateral GGO. Extensive Bronchiectasis. Scattered Pneumatoceles.	DAD with organization. Early Interstitial fibrosis. Microscopic Honeycombing. Pulmonary infarct.
TXC7	Extensive Bilateral Consolidations. Complete bilateral opacification. Small pleural effusions.	Interstitial Fibrosis with microscopic honeycombing. Occasional intravascular thrombi. Endothelial proliferation and endothelitis in left lung. Rare multinucleate giant cells. Foci of acute pneumonia. Left upper lobe shows more active interstitial fibrosis with many interstitial fibroblasts.
TXC8	Moderate multifocal patchy and confluent GGO and basilar predominant consolidations in both lungs. Superimposed mild interlobular septal thickening.	Alveolated lung parenchyma and a focus of small airway mucosa. Hyaline membrane formation is noted in all fragments with patchy acute interstitial pneumonia. No perivascular lymphoplasmacytic infiltrates diagnostic of acute rejection are identified.
TXC9	Lungs have small bilateral pleural effusions and extensive consolidation fill the lung fields. Small areas of aerated lung in the apices bilaterally filled with GGO.	Lung explant showed diffuse uniform alveolar septal thickening due to diffuse inflammation and fibrosis, overall consistent with organizing DAD bilaterally.
TXC10	Secretions are present in the central airways. Is ongoing organization throughout the lungs compared to prior examination, with substantially decreased extent of the multifocal airspace disease compared to prior exam. There is bronchial dilation and architectural distortion, indicative of ongoing organization. Small bilateral pleural effusions, partially loculated on the right.	Sections of the bilateral lungs show similar findings. The lung parenchyma shows diffuse interstitial fibrosis and mixed inflammation. There is focal organizing pneumonia. The majority of air spaces are filled with hemosiderin-laden macrophages or blood and focal mucous plugging is seen. Focal lymphoid aggregates are present. There is bilateral fibrous thickening of the pleura with focal acute inflammation. The bronchial margins show focal squamous metaplasia. Multiple benign lymph nodes are identified. No malignancy is identified.
TXC11	Bilateral diffuse airspace disease with extensive GGO and alveolar opacities in the upper lobes with consolidation and air bronchograms of the lower lobes. Relative to previous imaging the findings have significantly progressed likely related to multifocal pneumonia/ARDS. Trace pleural effusions. No pneumothorax.	Extensive interstitial fibrosis with patchy organizing diffuse alveolar damage, multifocal acute bronchitis, and bronchiolitis with adjacent pneumonia and peribronchiolar metaplasia. There is a small vessel thrombus seen in the left lung.
TXC12	Within the lungs, extensive consolidation throughout both lungs has increased/progressed. A small left apical pneumothorax is noted. There is no right apical pneumothorax or evidence of pneumomediastinum. There are no pleural effusions. The central airways are patent.	Prominent interstitial fibrosis with multifocal microscopic honeycomb pattern, type II pneumocyte hyperplasia, mucus plugs with acute inflammatory cells, diffuse chronic inflammatory infiltrate focal squamous metaplasia, extensive bronchiolar metaplasia, subpleural fibrosis, hemorrhage, and scattered calcium phosphate calcifications. There are numerous hemosiderin-laden and foamy macrophages within the airspaces. Foci of acute pneumonia and organizing pneumonia are also identified. Rare multinucleated cells are also seen. Medium size arteries show in some areas irregular intimal hyperplasia.
TXC13	Stigmata of ARDS cystic lung destruction and an upper lobe predominant distribution. There is overall decreasing consolidation in both lower lobes compared to previous examination. Peripheral bronchiectasis is again noted.	Both lungs show diffuse NSIP interstitial fibrosis pattern that most likely represents organized diffuse alveolar damage. There are foci of honeycombing and peribronchiolar metaplasia. There are scattered hemosiderin laden macrophages. Both lungs show extensive areas of calcification following a dendritic pattern.
TXC14	Severe extensive bilateral pulmonary infiltrates with air bronchograms are noted. Heart size is mildly enlarged.	Lung showed diffuse interstitial fibrosis and fibroblast proliferation and patch areas of necrosis and changes of diffuse alveolar damage w hyaline membrane formation. Hemosiderin filled macrophages in alveolar space w bronchiolar metaplasia of alveoli and squamous metaplasia.
TXC15	N/A	Sections show extensive diffuse interstitial fibrosis with areas of honeycombing and focal NSIP like pattern. There is extensive atelectasis. There is multifocal peribronchiolar metaplasia and deposition of hemosiderin-laden macrophages with fresh hemorrhage. The large caliber arteries show fibrous intimal thickening.

(Table 2 continues on next page)

CASE no.	CT Chest High resolution	Histopathology
(Continued from previous page)		
TXC16	Extensive airspace consolidation primarily posteriorly throughout the bilateral upper and lower lobes with air bronchograms and bronchiectasis. Minimal aeration of the lung bases. There is diffuse reticular thickening and GGO involving all segments of both lungs. Findings have significantly progressed from prior. No pleural effusion or pneumothorax. No lymphadenopathy.	Sections from both: right and left lungs show similar changes: There is uniform interstitial alveolar septal thickening due to young interstitial collagen. Some areas show collapse and occasional areas of mature collagen. In some areas, it is possible to see remnants of hyaline membrane admixed with inflammatory cells. Occasional isolated fibrin thrombi are seen in some small arteries. Granulomas or viral cytopathic effect is not identified.
TXC17	Extensive bilateral peripheral GGO and reticular opacity are reidentified with mild progression suspected mainly manifested as increased density of the affected areas, although this could be related to differences in inspiration. A thin rim of subpleural sparing is again suspected. There is traction bronchiectasis. No suspicious pulmonary nodules are identified, and there is no new airspace consolidation.	Both sides show interstitial fibrosis with spatial heterogeneity, extensive vascular margins are unremarkable. No granulomas or malignancy is identified. Sections of the native right lung show interstitial fibrosis with spatial heterogeneity, most prominent in the right middle and lower lobe. There is also extensive chronic inflammation, honeycombing, thickening of alveolar walls, fibroblastic foci, and reactive alveolar changes including type 2 pneumocyte hyperplasia. Mucus plugging and focal emphysematous change is seen. Smooth muscle hyperplasia is noted. Five benign lymph nodes are identified. The bronchial and vascular margins are unremarkable. No granulomas or malignancy is identified.
TXC18	Perivascular GGO and consolidative changes. Reticulation, architectural distortion, and traction bronchiectasis. LUL cavitary lesion.	Diffuse alveolar septal thickening with both cellular and fibrosis, consistent with NSIP pattern of injury. No significant vascular change. No pathological change in pleura.
TXC19	Diffuse GGO, reticulation, architectural distortion, interlobular septal thickening, bronchiectasis, and peripheral predominant cystic changes.	Advanced fibrosis and altered architecture with cystic change. Intimal thickening of pulmonary artery. Focal acute pleuritis noted.
TXC20	Extensive bilateral lung scarring with mild, relative sparing of the lung apices. Mild bronchiectasis is worst at the lung bases.	Chronic interstitial pneumonia with evolving features of end-stage lung disease. Findings compatible with post-inflammatory type scarring, but also show focal usual interstitial (UIP) and NSIP.
TXC21	Mild diffuse GGO, interstitial opacities, and bronchiectasis. These were noted to be unchanged from previous scans and likely scar/fibrosis from the previous COVID-19 pneumonia.	Diffuse interstitial fibrosis with features of organizing diffuse alveolar damage. Infarcts noted in the left upper lobe.
TXC22	Extensive pneumomediastinum, trace bilateral pneumothoraces, and extensive subcutaneous emphysema. GGO throughout both lungs, suspicious for acute respiratory distress syndrome.	End stage lung disease with diffuse alveolar damage and marked fibrosis.
TXC23	Low lung volumes with nonspecific bronchiectasis/honeycombing suggest scarring/interstitial lung disease with a mid and upper lobe predominance. Confluent GGO of the remainder of the lungs is nonspecific and may reflect pulmonary edema though active pneumonitis is a consideration.	Honeycombing and marked diffuse scarring. Diffuse interstitial fibrosis and bronchiectasis noted in both lungs.

Radiological and histological findings were not available for all patients. Histopathological evaluation of explanted lungs revealed diffuse alveolar damage (DAD) with overlapping acute, organizing, or fibrotic phases in most cases. Microscopic honeycombing was noted in multiple NR-COVID subjects. Significant chronic interstitial inflammation was noted in all patients. The pattern mimics interstitial lung disease (ILD) specifically non-specific interstitial pneumonia (NSIP). Diffuse ground glass opacities (GGO) with bronchiectasis were noted in a majority of patients. Some were also noted to have usual interstitial pneumonia (UIP).

Table 2: **Radiographic and pathological features.**

liquified infarcts with cystic changes along with organized vasculitis and is likely from complete occlusion of pulmonary arteries from endothelitis/intramural thrombosis. Some cases showed vasculopathy in arteries with active endothelitis. Overall, the pattern mimics interstitial lung disease (ILD)/ non-specific interstitial pneumonia (NSIP) pattern as noted on CT chest along with vascular changes in pulmonary arteries. Taken together, these results highlight the rapid and fatal progression of lung injury to the extent of requiring lung transplantation in both elderly and young patients with or without comorbidities. However, the mechanisms that lead to fulminant lung injury in NR-COVID-19 are not known.

Heightened fibrotic matrix deposition in NR-COVID-19

The macroscopic characteristics of explanted lungs from NR-COVID-19 patients show clear evidence of hepatization and gross anatomical remodeling in some cases (Fig. 1a). Approximately, 21/23 cases showed evidence of hepatization. High resolution computed tomography (HRCT) images demonstrate a clear reduction of gas exchange capacity and evidence of fibrosis (Fig. 1b). Masson's Trichome revealed a robust evidence of lung fibrosis in NR-COVID-19 patients (Fig. 1c). Most impactful was the young age of the patients affected many under their 5th decade of life (Fig. 1d). Lung fibrosis also progressed rapidly in this subset of NR-COVID-19 patients, where the development of lung injury to a state that a lung transplant was required for survival took 119 days (ranging from 55 to 211; Fig. 1e). Compared to the typical presentation of IPF that takes years. These results confirmed the development of a FLF phenotype in NR-COVID-19 that is fatal and requires lung transplantation. Intriguingly, a strong predominance of the patients identified as Hispanic (74%), in contrast with IPF, one of the most common causes of lung transplantation where

Caucasian males are overrepresented.[27] However, similar to fibrotic diseases such as IPF[27] and combined pulmonary fibrosis and emphysema,[28] 83% of cases were male (Fig. 1f).

Molecular signature of NR-COVID-19

We hypothesized that patients with NR-COVID-19 may present with a unique fibrotic signature. To study this, we utilized the predesigned Bio-Rad panel for Pulmonary Fibrosis and compared the readouts from NR-COVID-19 to control lung tissue. In this initial study, tissue samples from upper or lower lobes from the same NR-COVID-19 or control lung were utilized. A heat map demonstrated that all except 1 NR-COVID-19 lung sample clustered together (Fig. 2). In addition, no obvious clustering between upper or lower lobes was seen among control or NR-COVID-19 samples (Fig. 2). Our heatmap revealed increased gene expression among the top 10 altered genes and a tendency for reduced gene expression for the next 10. The individual data points for these results are shown in Fig. 3. Our results revealed a dominant increase in transcripts encoding for extracellular matrix (ECM) genes: collagen (COL)1A2, COL3A1, POST, TNC, VCAN but not SPP1 (Fig. 3a–f). Intriguingly, genes associated with the bone morphogenic protein (BMP) and TGF-β signaling pathways showed increased expression of GREM1, a BMP-signaling inhibitor, but no change in SMAD2 expression (Fig. 3g and h). Analysis of the remaining top 20 genes revealed increased expression for metalloproteinase (MMP) 2 and 3 but not MMP1 nor TIMP (Supplementary Fig. S1a–d). Elevated expression of CXCL12 and HTR2A in NR-COVID-19 were also

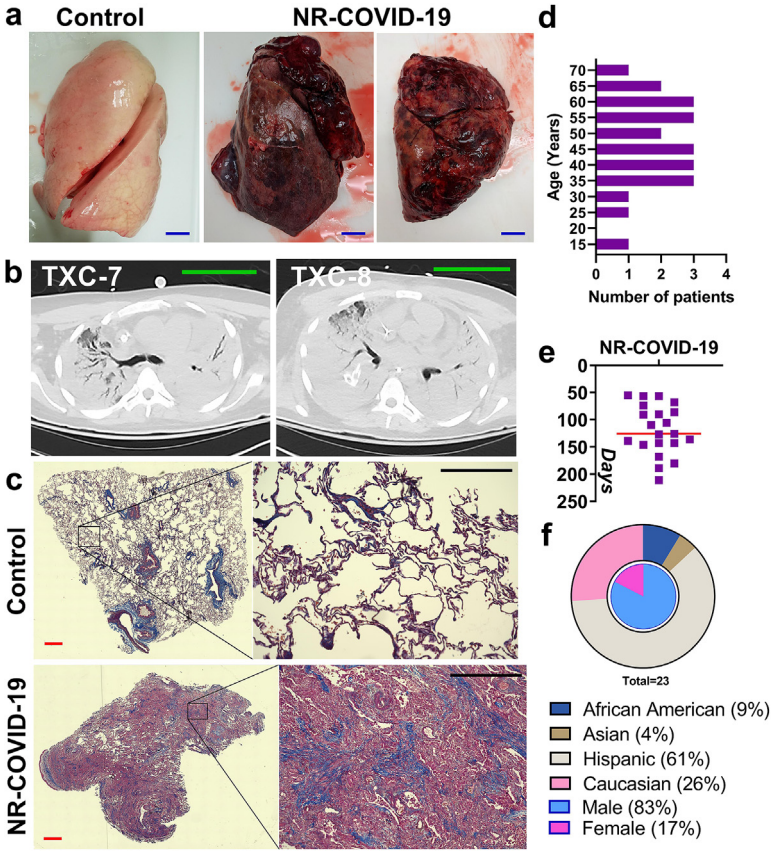

Fig. 1: **Macroscopic, radiologic, and histological findings in COVID-19 patients that require lung transplantation. a**) Macroscopic picture of a donor lung discarded for lung transplantation (control CTRL2), a COVID-19 lung explant (TXC7, TXC4) with non-resolvable (NR) COVID-19. **b**) High resolution CT (HRCT) image from two patients with NR-COVID-19. **c**) Masson's Trichome stained section showing the entire slide and a magnified window from a control (upper panel, CTRL2), and a NR-COVID-19 patient (bottom panel, TXC1). **d**) Frequency distribution histogram depicting the age of NR-COVID-19 patients who received a lung transplantation. **e**) Frequency distribution plot depicting the days between the first positive SARS-CoV-2 test and time of transplantation, the red line depicts the mean of 119 days. **f**) Pie-chart representing the different ethnicities and gender that make up our NR-COVID-19 transplant population percentages are shown in brackets. Blue scale bars in panel a represent 3 cm, green scale bars in panel b represent 10 cm, red scale bars in panel c represent 500 μm and black scale bars represent 100 μm.

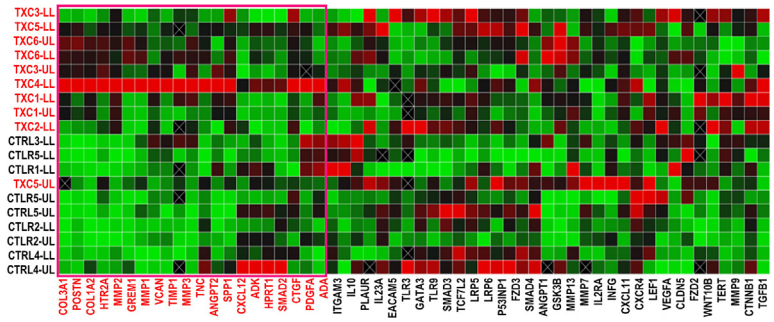

***Fig. 2:* Unbiased PCR Array findings.** Clustergram, for all samples, run using the Bio-Rad pulmonary fibrosis PCR Array. Control samples are in black font and NR-COVID-19 in red font. The gene names in red were significantly changed between control and NR-COVID-19. The colors indicate normalized expression using GAPDH and TBP as control genes. Green represents reduced expression whereas red represents increased expression levels.

identified (Supplementary Fig. S1e and f). No other genes were significantly altered between control and NR-COVID-19 (Supplementary Fig. S1g–l). Taken together these results point to a hyper-fibrotic response in NR-COVID-19 lungs.

Hyper-fibrotic response in NR-COVID-19

We next performed confirmatory RT-qPCR utilizing tissue derived from lower lobes only from control (N = 13), IPF (N = 11), and NR-COVID-19 (N = 23) lung tissues. These experiments revealed significantly elevated expression levels for the ECM genes COL1A2, COL2A1, COL3A1, and POSTN in IPF or NR-COVID-19 (Fig. 4a–d). COL1A2, COL3A1, and POSTN levels were most upregulated in NR-COVID-19 samples compared to control or IPF, whereas COL2A1 was predominantly elevated in IPF samples. No changes in TNC expression were identified, however VCAN mRNA levels appeared to be reduced in both IPF and NR-COVID-19 samples relative to controls (Fig. 4a–f). Consistent with increased POSTN mRNA levels we also report increased POSTN protein levels in both IPF and NR-COVID-19 samples (Fig. 4g); intriguingly, despite reduced VCAN transcripts our data show upregulated VCAN protein levels in some IPF and in all NR-COVID-19 samples (Fig. 4h). Expression levels for GREM1 (an endogenous inhibitor for BMPR2) SMAD2 transcripts revealed increased levels in IPF samples compared to control or NR-COVID-19 tissues (Fig. 4i and j). These results would suggest an increase in SMAD2,3 signaling and reduced SMAD1,5 responses in IPF samples compared to NR-COVID-19. Yet, strong evidence for TGF-β signaling in both IPF and NR-COVID-19 samples was evident in

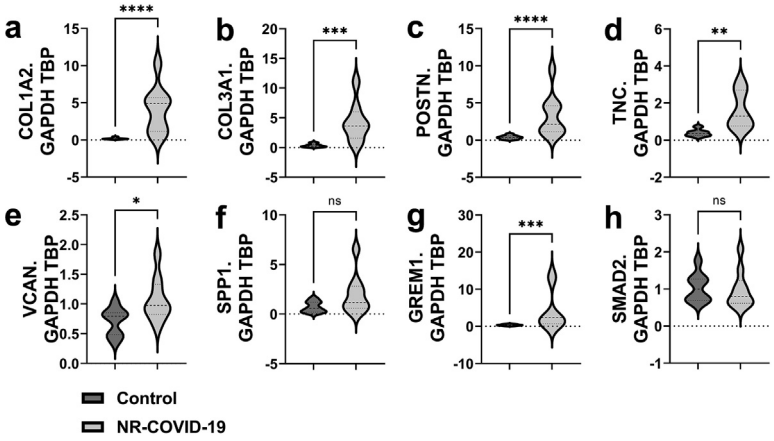

***Fig. 3:* Individual expression of PCR Array findings.** Expression levels for profibrotic genes: collagen (COL)1A2 (**a**), COL3A1 (**b**), Periostin (POSTN, **c**), Tenascin C (TNC, **d**), Versican (VCAN), osteopontin (SPP1, **f**), Gremlin 1 (GREM1, **g**) and SMAD2 (**h**) derived from the PCR Array data where TBP, GAPDH, ANGPT1, LRP5, and LRP6 were used as reference genes. Individual plots for each lung sample (upper or lower lobes) for each patient are plotted independently. Significance levels *P < 0.05 refers to comparisons between Control (dark grey, N = 10 from 5 individual lungs) and NR-COVID-19 (light grey, N = 13 from 7 individual lungs). Dashed lines represent the median and the dotted lines represent the upper and lower quartiles.

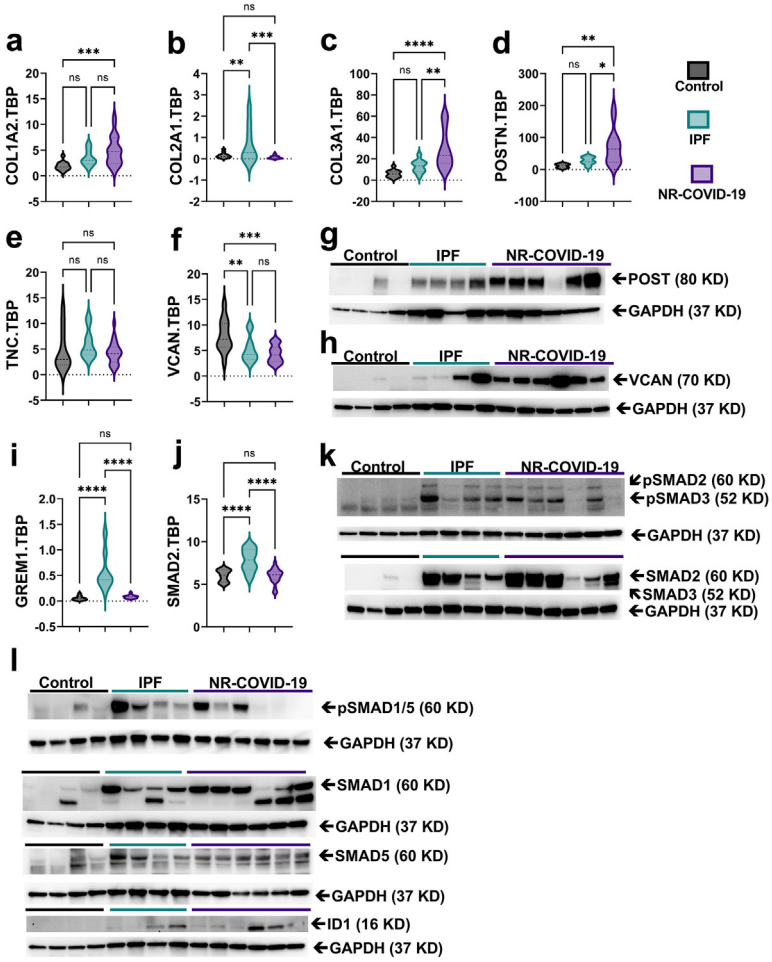

Fig. 4: **Confirmatory RT-PCR for extracellular matrix (ECM) constituents.** Transcript levels for collagen 1 A 2 (COL1A2, **a**), COL2A1 (**b**), COL3A1(**c**), periostin (POSTN, **d**). tenascin C (TNC, **e**), and versican (VCAN, **f**) using TBP as a reference gene. Western blot for POSTN and VCAN using GAPDH as a reference gene for control, IPF, and NR-COVID-19 samples (**g** and **h**). Transcript levels for Gremlin 1 (GREM1, **i**), SMAD2 (**j**) using TBP as a reference gene. Western blot for pSMAD 2,3; and SMAD2,3; using GAPDH as a reference gene for control, IPF, and NR-COVID-19 (**k**). Western blots for pSMAD 1,5; SMAD1; SMAD5 and ID1 using GAPDH as a reference gene for control, IPF, and NR-COVID-19 samples (**l**). Significance levels: *P < 0.05, **P < 0.01, ***P < 0.001, ****P < 0.0001, refers to One-way ANOVAs with the Benjamini, Krieger and Yekutieli post-hoc test between Control (grey, N = 13), IPF (teal, N = 11) and NR-COVID-19 (purple, N = 23). Dashed lines represent the median and the dotted lines represent the upper and lower quartiles.

Western blots for pSMAD2,3 and SMAD2,3 (Fig. 4k). Similarly, evidence for BMP signaling was evident in IPF and NR-COVID-19 samples per Western blots for pSMAD1,3, SMAD1, SMAD5, and ID1 showing a higher presence of these proteins in IPF and NR-COVID-19.

Increased CTHRC1 signals and KRT5/KRT8 in NR-COVID-19

Next, to identify the potential source of excess collagen production in NR-COVID-19 lungs, we evaluated expression levels of CTHRC1. CTHRC1+ cells have been associated with highly active pro-fibrotic fibroblasts in lung fibrosis[20] and expansion of this cell type has been detected in fatal COVID-19 ARDS.[19] Herein we reveal a significant increase in the transcript levels of CTHRC1 in IPF and NR-COVID-19 tissues compared to controls (Fig. 5a) consistent with increased protein levels (Fig. 5b). In severe injury models, activation of KRT5 in a lung progenitor cell[29] has been shown to be important following influenza or bleomycin exposure. These KRT5+ cells have been shown to proliferate and migrate to injured sites.[29] Further, recent studies have also identified a convergence of airway and alveolar stem cells to a KRT8+ transitional stem cell that persists in

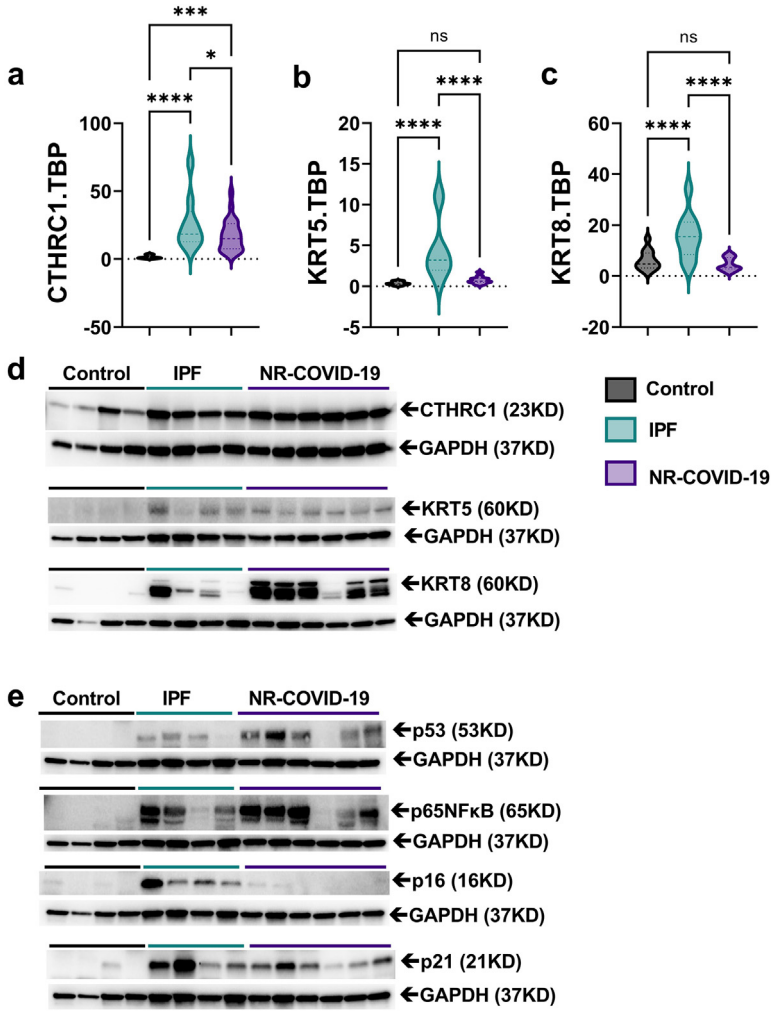

Fig. 5: **Elevated CTHRC1 and KRT5/KRT8 expression in NR-COVID-19.** Transcript levels for Collagen Triple Helix Repeat Containing 1(CTHRC1, **a**), cytokeratin 5 (KRT5, **b**), and KRT8 (**c**) using TBP as a reference gene. Western blots (**d**) for CTHRC1, KRT5, and KRT8 using GAPDH as a reference gene for control, IPF, and NR-COVID-19 samples. Western blots (**e**) for p53, p65 NFκB, p16, and p21 using GAPDH as a reference gene for control, IPF, and NR-COVID-19 samples. Significance levels: *P < 0.05, and ****P < 0.0001, refers to One-way ANOVAs with the Benjamini, Krieger, and Yekutieli post-hoc test between Control (grey, N = 13), IPF (teal, N = 11) and NR-COVID-19 (purple, N = 23). Dashed lines represent the median and the dotted lines represent the upper and lower quartiles.

lung fibrosis.[21] Thus, we determined whether KRT5 and KRT8 were upregulated in NR-COVID-19. Our experiments reveal increased transcript levels for KRT5 and KRT8 in IPF but not in NR-COVID-19 samples (Fig. 5b and c). Intriguingly, protein levels for KRT5 and KRT8 were elevated in both IPF and NR-COVID19 tissues, with stronger signals for KRT8 in NR-COVID-19 samples (Fig. 5d). Increased expression of KRT8 has been shown to be induced by p53 and NF-κB signaling,[21] in line with this, our results show increased signals for p53 and p65 NF-κB, in both IPF and NR-COVID-19 tissues (Fig. 5e). Assessment of the senescence markers p16 and p21 revealed increased signals for p16 in IPF samples only and elevated p21 in both IPF and NR-COVID-19 (Fig. 5e).

Localization studies for CTHRC1 revealed increased signals in cells that also expressed SMA within fibrotic foci (Fig. 6a). However, other cells positive for CTHRC1 were also detected (Fig. 6a). Staining for KRT5 revealed a dense layer of KRT5+ cells adjacent to fibrotic areas of the lung in NR-COVID-19 patients (Fig. 6b). Similar to KRT5, staining for KRT8 also revealed clusters of KRT8+ cells in NR-COVID-19 adjacent to fibrotic foci (Fig. 6c). Further staining for CTHRC1, KRT5, and KRT8 in IPF lung samples revealed evidence for positive CTHRC1, KRT5, and KRT8 cells close to fibrotic foci (Fig. 7). IHC in tissues

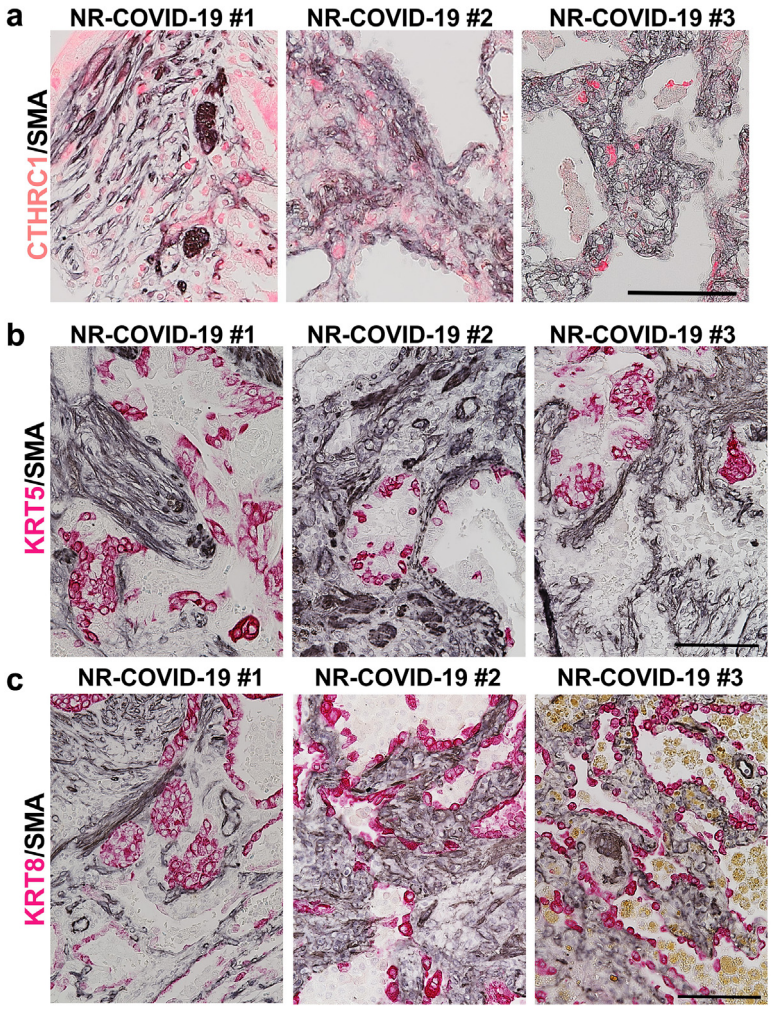

***Fig. 6:* Localization of CTHRC1, KRT5, and KRT8 signals in NR-COVID-19.** Double immunohistochemistry for CTHRC1, KRT5, or KRT8 and smooth muscle actin (SMA). **a**) Representative histological images from dual CTHRC1 and SMA signals from 3 distinct NR-COVID-19 patients denoting CTHRC1 adjacent to SMA expressing cells. Representative histological images from dual KRT5 and SMA signals (**b**) or dual KRT8/SMA (**c**) from 3 distinct NR-COVID-19 patients denoting KRT5 cells adjacent to SMA expressing cells and in the bronchiolization lung epithelium. Scale bar represents 50 μm.

from patients with Diffuse Alveolar Damage (DAD) revealed a lower level of expression for CTHRC1, KRT5, and KRT8 outside conducting airways where KRT5 and KRT8 levels are expected (Supplementary Fig. S2). Taken together, these results point to an expansion or recruitment of CTHRC1 and KRT5/KRT8 cells in NR-COVID-19 adjacent to fibrotic foci, that appear to be of similar or greater magnitude than IPF tissues. These observations underscore the aggressive fibroproliferative response in this subset of COVID-19 patients who require lung transplantation.

Discussion

Our results highlight the fulminant development of lung fibrosis in patients who were diagnosed with COVID-19 and required a lung transplant. Our patients were on average 47 years old and were transplanted 120 days after first diagnosis of SARS-CoV-2, similar to initial studies where lung transplantation was performed in severe COVID-19.[30] Clinically, our patient cohort mirrors previously reported findings[30] except for the fact that 8/23 patients for which we have thorough hospital course information from our cohort did not receive ECMO and the presence of endotheliitis and vasculopathy may reflect viral-induced endothelial cell damage.[31,32] An important difference with NR-COVID-19 patients with IPF is the fact that the majority of these patients were in their 3rd and 4th decade of life and identified as Hispanic, with only 26% identifying as Caucasian. This is contrary to IPF which is dominated by Caucasians in their 50s and 60s.[33] These potential

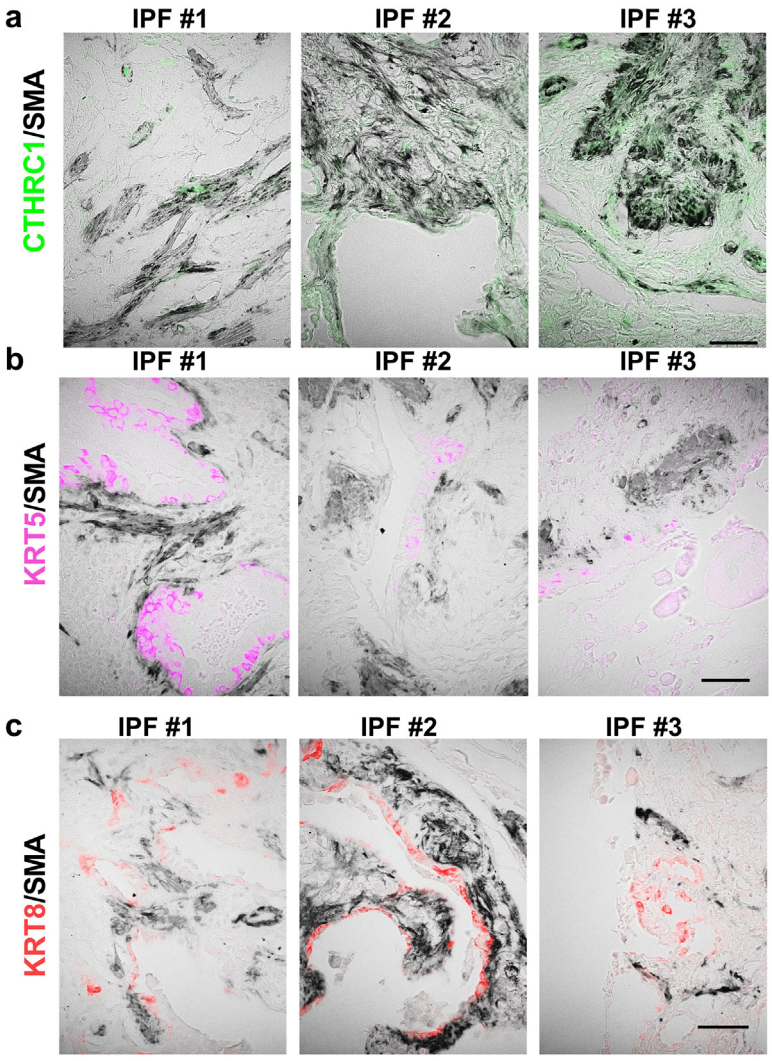

Fig. 7: **Localization of CTHRC1, KRT5, and KRT8 signals in IPF patients.** Double immunohistochemistry for CTHRC1, KRT5, or KRT8 and smooth muscle actin (SMA). **a**) Representative histological images from dual CTHRC1 and SMA signals from 3 distinct IPF patients denoting CTHRC1 adjacent to SMA expressing cells. Representative histological images from dual KRT5 and SMA signals (**b**) or dual KRT8/SMA (**c**) from 3 distinct IPF patients denoting KRT5 cells adjacent to SMA expressing cells. Scale bar represents 50 μm.

differences could be explained by socioeconomic factors disproportionately affecting Hispanics. Intriguingly, studies showing a protective effect of the IPF risk allele rs35705950 at MUC5B[34] (common in Caucasians) in severe COVID-19.[35]

Our unbiased approach revealed heightened expression levels of profibrotic genes in NR-COVID-19, underscoring the rapid development of lung fibrosis. These findings are consistent with prior studies identifying a pro-fibrotic cell population following scRNA studies and histopathological analysis that revealed similarities with IPF.[23] Comparative analysis of ECM gene expression for IPF and NR-COVID-19 samples in our study revealed a distinct fibrotic gene expression profile for NR-COVID-19 compared to IPF. IPF samples presented with a much more elevated expression of COL2A1 and more robust evidence for TGF-β signaling, as evidenced by mRNA and protein expression for GREM1 (mRNA only) and SMAD2,3 activation. However, NR-COVID-19 samples presented with a more pervasive increase in COL1A2, COL3A1, POSTN, and VCAN signals compared to IPF tissues. These results suggest potential differences in fibrotic gene expression and mechanisms in NR-COVID-19 compared to IPF. BMP signaling revealed variable expression of pSMAD 1,5, SMAD 1, and ID1 expression in both IPF and NR-COVID-19 samples. These differences could be attributed to the presence of vascular abnormalities such as

pulmonary hypertension, which could lead to reduced expression of p-SMAD1,5 as shown in IPF.[36] Vascular abnormalities have also been detected in COVID-19[31,32] and thus it is possible for these changes to remain present in NR-COVID-19. These findings are significant since little is known about the mechanisms that promote FLF in NR-COVID-19 and highlight potential differences with IPF.

Most strikingly is the increased expression of CTHRC1, KRT5, and KRT8 in NR-COVID-19. Herein, we report increased CTHRC1 expression levels and protein levels for CTHRC1. Histology revealed signals for CTHRC1 within SMA-expressing cells. These results are consistent with the identification of CTHRC1-expressing fibroblasts as a central cell involved in the production of collagen in lung fibrosis.[20] These results are also in line with scRNA-seq studies in fatal COVID-19 identifying the expression of CTHRC1 expressing cells.[19] Our studies also reveal an overwhelming expression of KRT5 and particularly KRT8 expressing cells in NR-COVID-19. Although enhanced expression of these cells was also identified in fatal COVID-19[19]; our results show that KRT5 and especially KRT8 positive cells are present adjacent to fibroblastic foci and in the bronchiolization of the lung epithelium (Supplemental IHC). These results are consistent with elevated KRT5 cells in IPF[37] and the notion of differentiation-arrested stem cell states in lung fibrosis expressing KRT8.[21] In line with this, we also report increased p53 and NF-κB activation.[21] Thus, it is conceivable that in NR-COVID-19, activation of pro-fibrotic mechanisms includes the recruitment of CTHRC1-expressing fibroblasts and KRT5/KRT8 epithelial cells that lead to FLF requiring transplantation within 119 days after a SARS-CoV-2 infection. Intriguingly, our results appear to point to a more pervasive expression of KRT8 cells in NR-COVID-19 lungs compared to IPF, this may be due to the early presentation of fibrosis following SARS-CoV-2 infection where lung transplantation was necessary within 120 days vs IPF where patients have progressively become worse over several years.

In contrast to previous studies[23,25,30,38,39] where all patients but 1 underwent ECMO, 12/17 patients from our cohort underwent ECMO. This is significant as increased time on mechanical ventilation[40] and stretch[41] have been associated with increased risk factors for lung fibrosis.[42] However, our data does not show differences in expression levels of pro-fibrotic markers between patients that received ECMO vs those that did not with the exception of TNC that was reduced in the ECMO group (Supplementary Fig. S3). These findings suggest that ECMO alone is unlikely to amplify fibrotic lung injury in NR-COVID-19.

We detected elevated levels of POSTN, a matricellular protein that binds to both ECM constituents and to cell surface receptors[43] in NR-COVID-19. In the context of lung fibrosis, several studies have identified increased circulating and tissue levels of POSTN in IPF.[44,45] POSTN has been postulated as a marker for disease progression in IPF[44–46] and it has been shown to promote lung fibrosis by interacting with type 1 collagen and FN1,[47] both of which are upregulated in our study. In addition, studies have also demonstrated a pro-fibrogenic effect of POSTN through its capacity to stimulate myofibroblast differentiation[48] and its cross-talk with TGF-β signaling.[49] Interestingly, increased levels of POSTN were also detected in a subtype of pro-fibrotic cells by scRNA-seq in COVID-19 that required lung transplantation[23]; and increased periostin was also detected in bronchoalveolar lavage fluid (BALF) from patients with critical COVID-19.[50]

Despite our IPF cohort representing patients with an average age of 51.8 years compared to the NR-COVID-19 (46.7) and control (42.8) groups, our data revealed robust evidence of senescence in IPF patients (elevated p16 and p21) levels compared to NR-COVID-19 and control samples. NR-COVID-19 samples showed no increase in p16 albeit elevated levels of p21. Intriguingly, p21 has been associated with the inactivation of DNA replication early in senescence and p16 with cellular differentiation programs that are turned on by senescent cells.[51] These results suggest that in our cohort, cell senescence may be at an earlier stage in NR-COVID-19 compared to IPF individuals of similar age, highlighting a potential role of cellular senescence in post SARS-CoV-2 fibrosis, as identified in IPF.[52]

Thus, taken together our results demonstrate a unique hyper-fibrotic phenotype in NR-COVID-19 that appears on average 120 days after testing positive for SARS-CoV-2 and is dominated by increased pro-fibrotic mediators and hyperexpression of CTHRC1, KRT5, and KRT8. Important differences with IPF include a much younger age of onset, a potentially unique fibrotic gene expression, and a predominance in Hispanic individuals. Caveats and limitations include the limited understanding regarding the mechanism that leads to the expansion of CTRHC1 and epithelial transitional cell lines in NR-COVID-19 in addition to potential interactions between fibroblasts and epithelial cells in this aggressive presentation of SARS-CoV-2 infection.

Contributors

S.S.K.J., A.P., Y.L., and H.K.-Q.: conducted experiments, acquired data, analyzed data, and wrote the manuscript. W.B., P.S., S.Y., P.S.G., X.Y., B.A., S.C., and N.W. conducted experiments, acquired data, and analyzed data. B.Z., L.M.B., and F.P.d.F. analyzed data and provided research material. S.S.K.J. and H.J.H. provided research material and help interpret clinical data. R.A.T. provided research material. H.K.E. and I.O.R. analyzed and interpreted data and provided reagents. S.S.K.J., S.Y., P.S.G. and H.K.-Q. accessed and verified the underlying data. H.K.-Q. serves as the guarantor of the study. All authors read and approved the final version of the manuscript.

Data sharing statement

Due to the nature of this research, to protect the participants' privacy and confidentiality, raw data are not shared publicly. Relevant data supporting the findings and conclusions of this study are available within the article and/or supplementary materials. Upon a justifiable

request, the share of de-identified data should be approved by the board of an investigational ethics committee.

Declaration of interests

All authors declare no conflict of interest except for HJH who served as speaker and advisory panel member for Boehringer Ingelheim for Nintedanib.

Acknowledgments

Kelli Wallen (MPH), for her help in proof-reading the manuscript. National Institutes of Health (NIH) Grants R01HL154720, R01DK122796, R01DK109574, R01HL133900, and Department of Defense (DoD) Grant W81XWH2110032 to H.K.E. NIH Grants: R01HL138510 and R01HL157100, DOD Grant W81XWH-19-1-0007, and American Heart Association Grant: 18IPA34170220 to H.K.-Q. American Heart Association: 19CDA34660279, American Lung Association: CA-622265, Parker B. Francis Fellowship, 1UL1TR003167–01 and The Center for Clinical and Translational Sciences, McGovern Medical School to X.Y.

Appendix A. Supplementary data

Supplementary data related to this article can be found at https://doi.org/10.1016/j.ebiom.2022.104351.

References

1 Grasselli G, Tonetti T, Protti A, et al. Pathophysiology of COVID-19-associated acute respiratory distress syndrome: a multicentre prospective observational study. *Lancet Respir Med*. 2020;8(12):1201–1208.
2 Wu C, Chen X, Cai Y, et al. Risk factors associated with acute respiratory distress syndrome and death in patients with coronavirus disease 2019 pneumonia in Wuhan, China. *JAMA Intern Med*. 2020;180(7):934–943.
3 Richardson S, Hirsch JS, Narasimhan M, et al. Presenting characteristics, comorbidities, and outcomes among 5700 patients hospitalized with COVID-19 in the New York City area. *JAMA*. 2020;323(20):2052–2059.
4 Williams GW, Berg NK, Reskallah A, Yuan X, Eltzschig HK. Acute respiratory distress syndrome: contemporary management and novel approaches during COVID-19. *Anesthesiology*. 2020;134(2):270–282.
5 CDC. *COVID-19 pandemic planning scenarios*. 2020.
6 Ware LB, Matthay MA. The acute respiratory distress syndrome. *N Engl J Med*. 2000;342(18):1334–1349.
7 Thompson BT, Chambers RC, Liu KD. Acute respiratory distress syndrome. *N Engl J Med*. 2017;377(6):562–572.
8 Ranieri VM, Rubenfeld GD, Thompson BT, et al. Acute respiratory distress syndrome: the Berlin definition. *JAMA*. 2012;307(23):2526–2533.
9 Eltzschig HK, Carmeliet P. Hypoxia and inflammation. *N Engl J Med*. 2011;364(7):656–665.
10 Le TT, Berg NK, Harting MT, Li X, Eltzschig HK, Yuan X. Purinergic signaling in pulmonary inflammation. *Front Immunol*. 2019;10:1633.
11 Williams GW, Berg NK, Reskallah A, Yuan X, Eltzschig HK. Acute respiratory distress syndrome. *Anesthesiology*. 2021;134(2):270–282.
12 Lee LK, Medzikovic L, Eghbali M, Eltzschig HK, Yuan X. The role of MicroRNAs in acute respiratory distress syndrome and sepsis, from targets to therapies: a narrative review. *Anesth Analg*. 2020;131(5):1471–1484.
13 Yuan X, Lee JW, Bowser JL, Neudecker V, Sridhar S, Eltzschig HK. Targeting hypoxia signaling for perioperative organ injury. *Anesth Analg*. 2018;126(1):308–321.
14 Burnham EL, Janssen WJ, Riches DW, Moss M, Downey GP. The fibroproliferative response in acute respiratory distress syndrome: mechanisms and clinical significance. *Eur Respir J*. 2014;43(1):276–285.
15 Hui DS, Joynt GM, Wong KT, et al. Impact of severe acute respiratory syndrome (SARS) on pulmonary function, functional capacity and quality of life in a cohort of survivors. *Thorax*. 2005;60(5):401–409.
16 Spagnolo P, Balestro E, Aliberti S, et al. Pulmonary fibrosis secondary to COVID-19: a call to arms? *Lancet Respir Med*. 2020;8(8):750–752.
17 Shi H, Han X, Jiang N, et al. Radiological findings from 81 patients with COVID-19 pneumonia in Wuhan, China: a descriptive study. *Lancet Infect Dis*. 2020;20(4):425–434.
18 Xu J, Xu X, Jiang L, Dua K, Hansbro PM, Liu G. SARS-CoV-2 induces transcriptional signatures in human lung epithelial cells that promote lung fibrosis. *Respir Res*. 2020;21(1):182.
19 Melms JC, Biermann J, Huang H, et al. A molecular single-cell lung atlas of lethal COVID-19. *Nature*. 2021;595(7865):114–119.
20 Tsukui T, Sun KH, Wetter JB, et al. Collagen-producing lung cell atlas identifies multiple subsets with distinct localization and relevance to fibrosis. *Nat Commun*. 2020;11(1):1920.
21 Strunz M, Simon LM, Ansari M, et al. Alveolar regeneration through a Krt8+ transitional stem cell state that persists in human lung fibrosis. *Nat Commun*. 2020;11(1):3559.
22 Zuo W, Zhang T, Wu DZ, et al. p63(+)Krt5(+) distal airway stem cells are essential for lung regeneration. *Nature*. 2015;517(7536):616–620.
23 Bharat A, Querrey M, Markov NS, et al. Lung transplantation for patients with severe COVID-19. *Sci Transl Med*. 2020;12(574).
24 Cypel M, Keshavjee S. When to consider lung transplantation for COVID-19. *Lancet Respir Med*. 2020;8(10):944–946.
25 Croci GA, Vaira V, Trabattoni D, et al. Emergency lung transplantation after COVID-19: immunopathological insights on two affected patients. *Cells*. 2021;10(3).
26 Garcia-Morales LJ, Chen NY, Weng T, et al. Altered hypoxic-adenosine axis and metabolism in group iii pulmonary hypertension. *Am J Respir Cell Mol Biol*. 2016;54(4):574–583.
27 Laporta Hernandez R, Aguilar Perez M, Lázaro Carrasco MT, Ussetti Gil P. Lung transplantation in idiopathic pulmonary fibrosis. *Med Sci (Basel, Switzerland)*. 2018;6(3):68.
28 Collum SD, Molina JG, Hanmandlu A, et al. Adenosine and hyaluronan promote lung fibrosis and pulmonary hypertension in combined pulmonary fibrosis and emphysema. *Dis Model Mech*. 2019;12(5):dmm038711.
29 Vaughan AE, Brumwell AN, Xi Y, et al. Lineage-negative progenitors mobilize to regenerate lung epithelium after major injury. *Nature*. 2015;517(7536):621–625.
30 Bharat A, Machuca TN, Querrey M, et al. Early outcomes after lung transplantation for severe COVID-19: a series of the first consecutive cases from four countries. *Lancet Respir Med*. 2021;9(5):487–497.
31 Karmouty-Quintana H, Thandavarayan RA, Keller SP, Sahay S, Pandit LM, Akkanti B. Emerging mechanisms of pulmonary vasoconstriction in SARS-CoV-2-induced acute respiratory distress syndrome (ARDS) and potential therapeutic targets. *Int J Mol Sci*. 2020;21(21):8081.
32 Potus F, Mai V, Lebret M, et al. Novel insights on the pulmonary vascular consequences of COVID-19. *Am J Physiol Lung Cell Mol Physiol*. 2020;319(2):L277–L288.
33 Lederer DJ, Martinez FJ. Idiopathic pulmonary fibrosis. *N Engl J Med*. 2018;378(19):1811–1823.
34 Seibold MA, Wise AL, Speer MC, et al. A common MUC5B promoter polymorphism and pulmonary fibrosis. *N Engl J Med*. 2011;364(16):1503–1512.
35 Fadista J, Kraven LM, Karjalainen J, et al. Shared genetic etiology between idiopathic pulmonary fibrosis and COVID-19 severity. *EBioMedicine*. 2021;65:103277.
36 Chen NY, Collum SD, Luo F, et al. Macrophage bone morphogenic protein receptor 2 depletion in idiopathic pulmonary fibrosis and group III pulmonary hypertension. *Am J Physiol Lung Cell Mol Physiol*. 2016;311(2):L238–L254.
37 Kathiriya JJ, Wang C, Zhou M, et al. Human alveolar type 2 epithelium transdifferentiates into metaplastic KRT5(+) basal cells. *Nat Cell Biol*. 2022;24(1):10–23.
38 Chen JY, Qiao K, Liu F, et al. Lung transplantation as therapeutic option in acute respiratory distress syndrome for coronavirus disease 2019-related pulmonary fibrosis. *Chin Med J*. 2020;133(12):1390–1396.
39 Lang C, Jaksch P, Hoda MA, et al. Lung transplantation for COVID-19-associated acute respiratory distress syndrome in a PCR-positive patient. *Lancet Respir Med*. 2020;8(10):1057–1060.
40 Thille AW, Esteban A, Fernández-Segoviano P, et al. Chronology of histological lesions in acute respiratory distress syndrome with diffuse alveolar damage: a prospective cohort study of clinical autopsies. *Lancet Respir Med*. 2013;1(5):395–401.

41 Heise RL, Stober V, Cheluvaraju C, Hollingsworth JW, Garantziotis S. Mechanical stretch induces epithelial-mesenchymal transition in alveolar epithelia via hyaluronan activation of innate immunity. *J Biol Chem*. 2011;286(20):17435–17444.

42 Albert RK, Smith B, Perlman CE, Schwartz DA. Is progression of pulmonary fibrosis due to ventilation-induced lung injury? *Am J Respir Crit Care Med*. 2019;200(2):140–151.

43 O'Dwyer DN, Moore BB. The role of periostin in lung fibrosis and airway remodeling. *Cell Mol Life Sci*. 2017;74(23):4305–4314.

44 Okamoto M, Hoshino T, Kitasato Y, et al. Periostin, a matrix protein, is a novel biomarker for idiopathic interstitial pneumonias. *Eur Respir J*. 2011;37(5):1119–1127.

45 Naik PK, Bozyk PD, Bentley JK, et al. Periostin promotes fibrosis and predicts progression in patients with idiopathic pulmonary fibrosis. *Am J Physiol Lung Cell Mol Physiol*. 2012;303(12):L1046–L1056.

46 Ohta S, Okamoto M, Fujimoto K, et al. The usefulness of monomeric periostin as a biomarker for idiopathic pulmonary fibrosis. *PLoS One*. 2017;12(3):e0174547.

47 Kudo A. Periostin in fibrillogenesis for tissue regeneration: periostin actions inside and outside the cell. *Cell Mol Life Sci*. 2011;68(19):3201–3207.

48 Ashley SL, Wilke CA, Kim KK, Moore BB. Periostin regulates fibrocyte function to promote myofibroblast differentiation and lung fibrosis. *Mucosal Immunol*. 2017;10(2):341–351.

49 Nanri Y, Nunomura S, Terasaki Y, et al. Cross-talk between transforming growth factor-β and periostin can be targeted for pulmonary fibrosis. *Am J Respir Cell Mol Biol*. 2020;62(2):204–216.

50 Zeng HL, Chen D, Yan J, et al. Proteomic characteristics of bronchoalveolar lavage fluid in critical COVID-19 patients. *FEBS J*. 2021;288(17):5190–5200.

51 Stein GH, Drullinger LF, Soulard A, Dulić V. Differential roles for cyclin-dependent kinase inhibitors p21 and p16 in the mechanisms of senescence and differentiation in human fibroblasts. *Mol Cell Biol*. 1999;19(3):2109–2117.

52 Schafer MJ, White TA, Iijima K, et al. Cellular senescence mediates fibrotic pulmonary disease. *Nat Commun*. 2017;8:14532.